catalysts

MDPI

Article

Electrochemically Obtained TiO_2/Cu_xO_y Nanotube Arrays Presenting a Photocatalytic Response in Processes of Pollutants Degradation and Bacteria Inactivation in Aqueous Phase

Magda Kozak [1,*], Paweł Mazierski [1], Joanna Żebrowska [2], Marek Kobylański [1], Tomasz Klimczuk [3], Wojciech Lisowski [4], Grzegorz Trykowski [5], Grzegorz Nowaczyk [6] and Adriana Zaleska-Medynska [1]

1 Department of Environmental Technology, Faculty of Chemistry, University of Gdansk, 80-308 Gdansk, Poland; pawel.mazierski@phdstud.ug.edu.pl (P.M.); marek.kobylanski@phdstud.ug.edu.pl (M.K.); adriana.zaleska@ug.edu.pl (A.Z.-M.)
2 Department of Molecular Biotechnology, Faculty of Chemistry, University of Gdansk, 80-308 Gdansk, Poland; joanna.zebrowska@ug.edu.pl
3 Faculty of Applied Physics and Mathematics, Gdansk University of Technology, 80-233 Gdansk, Poland; tomek@mif.pg.gda.pl
4 Institute of Physical Chemistry, Polish Academy of Sciences, 01-224 Warsaw, Poland; wlisowski@ichf.edu.pl
5 Faculty of Chemistry, Nicolaus Copernicus University, 87-100 Torun, Poland; tryki@umk.pl
6 NanoBioMedical Centre, Adam Mickiewicz University, Umultowska 85, 61-614 Poznan, Poland; nowag@amu.edu.pl
* Correspondence: magda.kozak@ug.edu.pl; Tel.: +48-58-523-5159

Received: 15 May 2018; Accepted: 2 June 2018; Published: 5 June 2018

Abstract: TiO_2/Cu_xO_y nanotube (NT) arrays were synthesized using the anodization method in the presence of ethylene glycol and different parameters applied. The presence, morphology, and chemical character of the obtained structures was characterized using a variety of methods—SEM (scanning electron microscopy), XPS (X-ray photoelectron spectroscopy), XRD (X-ray crystallography), PL (photoluminescence), and EDX (energy-dispersive X-ray spectroscopy). A p-n mixed oxide heterojunction of Ti-Cu was created with a proved response to the visible light range and the stable form that were in contact with Ti. TiO_2/Cu_xO_y NTs presented the appearance of both Cu_2O (mainly) and CuO components influencing the dimensions of the NTs (1.1–1.3 µm). Additionally, changes in voltage have been proven to affect the NTs' length, which reached a value of 3.5 µm for $Ti_{90}Cu_{10}$_50V. Degradation of phenol in the aqueous phase was observed in 16% of $Ti_{85}Cu_{15}$_30V after 1 h of visible light irradiation ($\lambda > 420$ nm). Scavenger tests for phenol degradation process in presence of NT samples exposed the responsibility of superoxide radicals for degradation of organic compounds in Vis light region. Inactivation of bacteria strains *Escherichia coli* (*E. coli*), *Bacillus subtilis* (*B. subtilis*), and *Clostridium* sp. in presence of obtained TiO_2/Cu_xO_y NT photocatalysts, and Vis light has been studied showing a great improvement in inactivation efficiency with a response rate of 97% inactivation for *E. coli* and 98% for *Clostridium* sp. in 60 min. Evidently, TEM (transmission electron microscopy) images confirmed the bacteria cells' damage.

Keywords: heterogeneous photocatalysis; TiO_2/Cu_2O nanotubes; anodization; nanomaterials fabrication; removal of microbiological pollutants

1. Introduction

Processes connected with the photocatalysis phenomenon are in area that is receiving great attention nowadays. Once we add nanomaterials to this combination, we will produce an interesting mix that not only scientists but also industry have been paying attention to lately. The main reason for this interest is the scope of application—i.e., the healthy nature of the environmental engineering and car industries.

Intensive studies on nanomaterials—research on properties, attempts to reduce their size or modifications—lead to the extension of the application possibilities. In recent years, more attention has been directed towards transformation processes that involve a light source—i.e., solve energy and pollution problems in the presence of semiconductors (photocatalysts). One of the semiconductors, considered as the most attractive photocatalyst in previous research, is TiO_2, which is characterized by a wide range of advantages, i.e., high chemical stability and relatively low price, and it is not toxic. It has been confirmed that it is applicable to the degradation of pollutants in both the gaseous and liquid phases [1,2], as well as in many different areas such as CO_2 reduction [3], water splitting [4], or antibacterial activity [5]. There is also one main disadvantage of TiO_2 photocatalysts, which is their minimal energy value (Eg, c.a 3.2 eV), which is necessary for the electron excitation that needed to generate holes in the valence band and carry on photocatalytic reactions. This value corresponds to 388 nm, so it can be activated in the UV irradiation range (300–380 nm), which really limits its applications [6].

The limitations have led to worldwide research focusing on TiO_2 modifications to extend its activity to the range of light irradiation of the Vis, such as sensitization with a semiconductor with a narrow band gap, metal ion doping, or nonmetal doping or dye sensitization [7]. These processes not only increase the activity but also modify the active surface area. There are two approaches in terms of the nanofabrication process: "top-down" and "bottom-up." The first represents the idea of using larger structures, which can be further controlled in the nanoscale, whereas the second includes the miniaturization of components with the self-assembly process. There are a variety of forms of modified nanostructures—nanoparticles, nanotubes (NTs), nanosheets, or nanocubes obtained using many methods such as electrodeposition [6], self-assembly examples, atomic layer deposition, or anodization [8–10].

Anodization of titanium and its alloys was performed in many environments [3,11], but modification of Ti alloys with this method was not so common. During the oxidation process, a big influence on the results of the experiment had some parameters such as applied voltage, the composition of the electrolyte, or the time of the process [12]. The anodic growth of compact oxides in metal surfaces and the formation of tubes are governed by a competition between anodic oxide formation and chemical dissolution of the oxide as a soluble fluoride complex. In 2001, Grimes et al. first reported the influence of hydrofluoric (HF) acid in the anodic oxidation process on the porosity of the titanium NT arrays [13]. It is proved that longer NTs are formed in electrolytes based on organic compounds like ethylene glycol or glycerol. Studies on literature show that usage of viscous solvents for anodization results in smooth wall structures of the NTs [14,15].

One promising aspect of TiO_2 modification is its ability to combine with Cu, including Cu_2O and CuO species, which can function as an electron mediator to widen the wavelength region for absorption [16]; however, Cu is not stable in terms of nano-scale size [17]. Furthermore, Cu_2O is also promising with regard to the formation of p-n heterojunctions with TiO_2 [18], which can lead to the improvement of the modified photocatalysts features. It was already reported that photocatalysts containing titanium and copper have the ability to cause pollutant degradation [19,20]; what is more, there is great potential in these materials in terms of inactivation of bacteria that has studied since 1985. Metsunga et al. were among the pioneers who studied the application of titanium dioxide (TiO_2) as a promising photocatalyst in terms of antimicrobial reactions [21]. Copper possesses high antimicrobial features [22] with the potential for drug degradation [23] and, due to lower toxicity, price, and increased cytocompatibility [24], it is more favorable than silver or gold. This is the

reason why it has been more intensively studied among other catalysts nowadays. Cu and TiO_2 combinations were studied in different modifications including photodeposition of copper [25], microwave co-precipitation technique [26], layer films [27], alloy rods [28], nanocrystals [19], composite coating on wooden substrate [29], copper decorated TiO_2 nanorods [30], combination of magnetron sputtering and annealing treatment [31], doped nanoparticles [32] or radiolytic deposition of copper species at the surface of TiO_2 nanotubes [33]. However, properties of nanostructures containing copper obtained *via* anodic oxidation using alloys are still rather unknown, and very little research has been undertaken to understand the quantity influence of copper in the Cu-TiO_2 nanostructured composite regarding the photocatalytic activities of Cu-doped TiO_2. Furthermore, the influence of different parameters on oxidation processes such as voltage, time, and electrolyte composition has not been fully studied yet. In view of this, in this work, it was decided to extend knowledge about the anodized Ti-Cu alloys while considering different parameters of the process. Moreover, the impact of anodized Ti-Cu alloys on bacteria inactivation (*E. coli, B. subtilis, Clostridium* sp.) in Vis light was investigated for the first time. The expected outcomes are as follows: (a) the anodic oxidation of Ti-Cu alloys will form TiO_2 NT arrays in various production conditions, (b) TiO_2/Cu_xO_y will show increased activity under Vis light, and (c) TiO_2/Cu_xO_y will present intense bacteria inactivation features.

2. Results and Discussion

2.1. Morphology and Formation of TiO_2/Cu_xO_y NTs

The surface morphology of obtained TiO_2/Cu_xO_y NTs was determined by SEM (scanning electron microscopy) and is presented in Figure 1a–e, while SEM images of references samples, namely, pristine TiO_2, are displayed in Figure S1 (Supplementary Materials). The upper layer of NTs remains unveiled, and only a small amount of initial barrier layer is visible, which suggests that cleaning the surface of samples after anodization in an ultrasonic bath was effective. Characteristic dimensions of NTs such as length, diameter, and wall thickness were calculated based on SEM images and are gathered in Table 1. Among the TiO_2/Cu_xO_y NTs, the length of tubes and external diameter varied from 1.1 to 3.5 µm and 83–98 nm, respectively, indicating that the shape of NTs strictly depends on applied voltage during anodization process and amount of Cu in the Ti-Cu alloys. In general, the length of all TiO_2/Cu_xO_y NTs is shorter than pristine TiO_2 NTs prepared from Ti foil under the same anodization conditions. Additionally, the length TiO_2/Cu_xO_y NTs decreased with the increase of Cu content in the Ti-Cu alloy. These phenomena have already been observed for the anodization of titanium alloys [34,35] and can be ascribed to the accelerated dissolution of TiO_2/Cu_xO_y NTs [28,34].

As will be described later (in XPS (X-ray photoelectron spectroscopy) part) by anodizing Ti-Cu alloys, we obtained p-n heterojunction consisting of TiO_2 NTs and Cu_xO_y species, in which Cu species appear in the form of Cu_2O (mostly) and CuO. Based on TEM image depicted in Figure 1f, we can conclude that Cu_xO_y species are evenly spaced along the NTs, and no nanoparticles formation was observed. On the other hand, the formation of copper oxides inside TiO_2 NTs at various oxidation states (Cu^{1+} and Cu^{2+}) can be represented by the following reactions [36,37]:

$$Cu - e^- \rightarrow Cu^+, 2Cu^+ + 2OH^- \rightarrow Cu_2O + H_2O \quad (1)$$

$$Cu - 2e^- \rightarrow Cu^{2+}, Cu^{2+} + 2OH^- \rightarrow CuO + H_2O \quad (2)$$

These reactions occur simultaneously with the formation of TiO_2, which can be represented as

$$Ti + 2H_2O \rightarrow TiO_2 + 4H^+ + 4e^- \quad (3)$$

$$TiO_2 + 4H^+ + 6F^- \rightarrow TiF_6^{2-} + 2H_2O \quad (4)$$

Reaction (4) affects the anodization process and is responsible for the growth of TiO_2 in the form of NTs [38,39].

Table 1. Sample labels, preparation conditions, NTs dimensions (based on SEM measurements), and Cu content (based on EDX (Energy-dispersive X-ray spectroscopy)).

Sample Label	Material of Working Electrode	Anodization Voltage (V)	External Diameter (nm)	Tubes Length (μm)	Wall Thickness (nm)	Cu Content (wt.%)
Ti_30V	Ti foil	30	80	1.5	10	-
Ti_40V		40	100	3.0	13	-
Ti_50V		50	120	6.0	18	-
$Ti_{95}Cu_5$_30V	Ti(95%)/Cu(5%) alloy	30	85	1.3	12	3.57
$Ti_{90}Cu_{10}$_30V	Ti(90%)/Cu(10%) alloy	30	88	1.2	11	6.20
$Ti_{85}Cu_{15}$_30V	Ti(85%)/Cu(15%) alloy	30	83	1.1	15	9.45
$Ti_{90}Cu_{10}$_40V	Ti(90%)/Cu(10%) alloy	40	98	2.5	14	6.25
$Ti_{90}Cu_{10}$_50V	Ti(90%)/Cu(10%) alloy	50	97	3.5	14	3.44

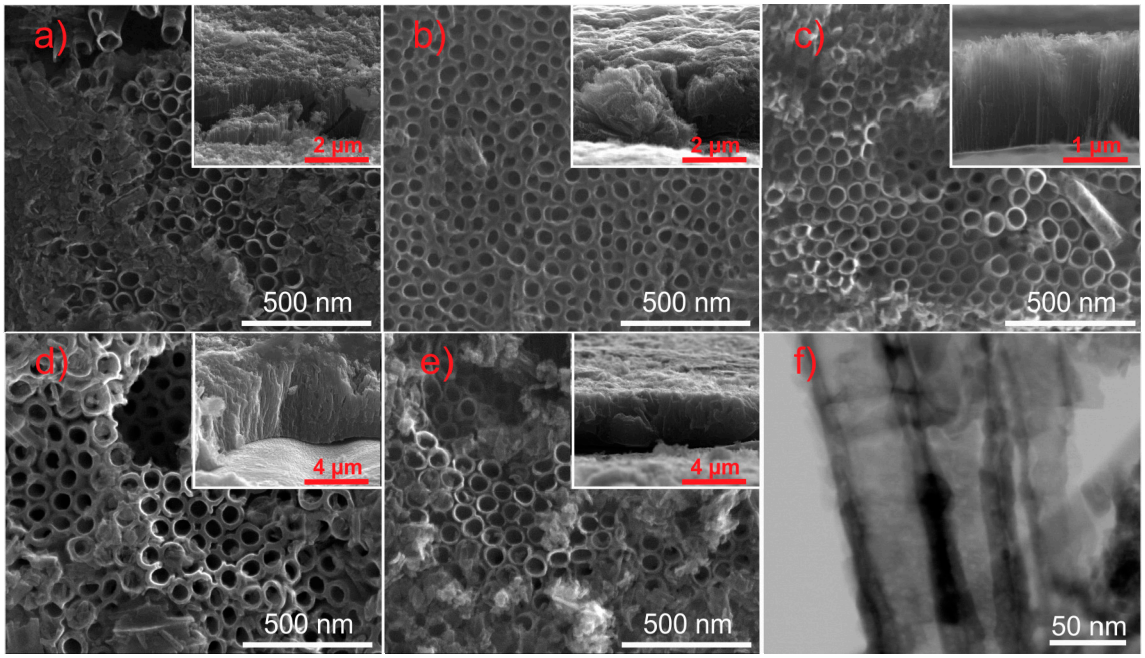

Figure 1. Top-view and cross-sectional SEM images of $Ti_{95}Cu_5$_30V (**a**), $Ti_{90}Cu_{10}$_30V (**b**), $Ti_{85}Cu_{15}$_30V (**c**), $Ti_{90}Cu_{10}$_40V (**d**), $Ti_{90}Cu_{10}$_50V (**e**) samples, and TEM image of $Ti_{95}Cu_5$_30V (**f**).

2.2. XRD Analysis

Phase composition of the tested samples was checked by using powder X-ray diffractometer (X'Pert Pro MPD, PANalytical, Almelo, The Netherlands). Figure 2 details diffraction patterns for Ti-Cu alloys after the anodic oxidation process. The patterns for Ti anodized samples are in Table S1 and Figure S2 (supplementary materials). The experimental data and refined model (LeBail) are represented by circles and a solid red line, respectively. The sets of vertical bars show expected positions for TiO_2—anatase (black), Ti (red), and $CuTi_2$ alloy (olive). The Miller indices for the anatase are shown in panel (d). The strongest reflection (101) is observed at around 25.3 deg. Ti foil is always observed with the strongest reflection at 40.3 deg. Foils with Cu concentration 10% and 15% reveal presence of $CuTi_2$ alloy—clearly seen by growing reflection near 16.6 deg. (Figure 2a,b). Interestingly, a relative signal of $CuTi_2$ is weaker for $Ti_{90}Cu_{10}$ samples anodized in 40V and 50V, compared to the one anodized in 30 V ($Ti_{90}Cu_{10}$_30V). It is likely caused by thicker film of anatase on the surface for $Ti_{90}Cu_{10}$_40V and $Ti_{90}Cu_{10}$_50V. We do not observe neither Cu metal, nor Cu oxides.

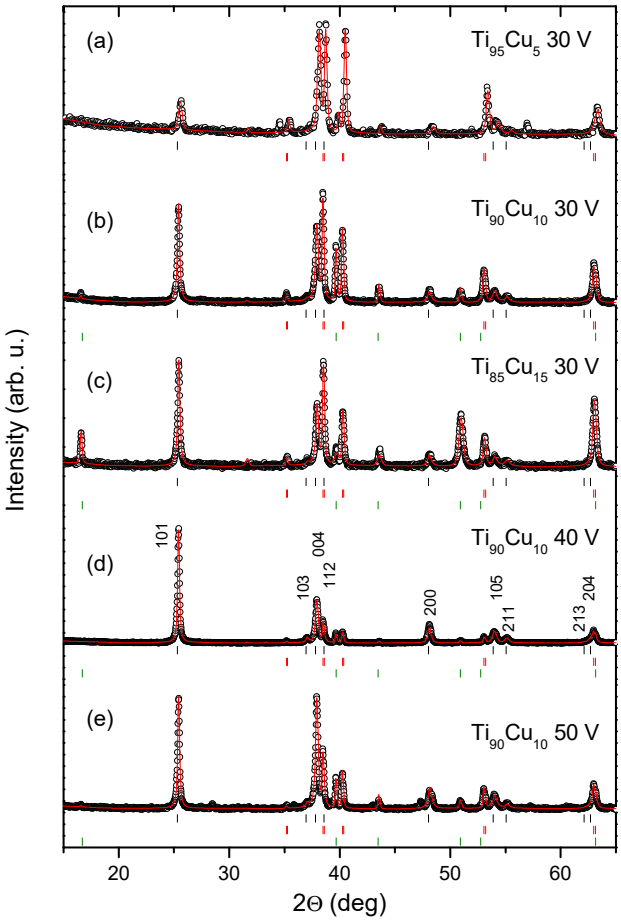

Figure 2. X-ray diffraction patterns for Ti-Cu alloys. A red solid line is a LeBail fit to the experimental data (open circles). Vertical bars represent positions of expected Bragg peaks for (from top): TiO_2—anatase (black), Ti (red), and $CuTi_2$ alloy (olive), respectively.

More qualitative results were obtained by using LeBail refinement. Table S1 contains obtained lattice parameters for TiO_2—anatase (tetragonal I41/amd, ICSD code: 063711), Ti—metal (hexagonal P63/mmc, ICSD code: 076265), and $CuTi_2$ (tetragonal I4/mmm, ICSD code: 015807) compounds. A corrected full width at half maximum (FWHM) of the strongest (101) anatase reflection was used for calculations of the average crystallite size using the Scherrer equation. The estimated size is between 250 Å and 460 Å for $Ti_{95}Cu_5$_30V and Ti_{90}Cu10_50V, respectively. However, because of complexity of

studied photocatalysts, presence of three oxides (TiO_2, Cu_2O, CuO), and different wall thickness of NTs, it is hard to obtain more information about the crystallite size. There is no obvious change of the anatase lattice parameters with the increasing voltage. The a and c parameters for Ti_30V, Ti_40V, and Ti_50V, as well as for $Ti_{90}Cu_{10}$_30V, $Ti_{90}Cu_{10}$_40V, and $Ti_{90}Cu_{10}$_50V series, remain almost the same. However, for the samples anodized in 30V, with different Cu content, there is increase in both a and c values. It is reflected also by increase in unit cell volume from 136.0 $Å^3$ ($Ti_{95}Cu_5$_30V) to 136.6 $Å^3$ ($Ti_{90}Cu_{10}$_30V) and 136.0 $Å^3$ ($Ti_{85}Cu_{15}$_30V). Higher Cu concentration is likely responsible for larger crystallite size: 250 Å, 360 Å, and 390 Å for 5%, 10%, and 15% Cu, respectively.

2.3. XPS Analysis

Elemental composition (in at.%) in the surface layer of Cu-modified TiO_2 NTs was evaluated by XPS analysis and reported in Table 2 and Table S2. Detection of Cu in addition to Ti and O confirm the effective modification of this element in all TiO_2 NTs. Carbon, nitrogen, and fluorine species were also detected. Results obtained in different studies by our group and also knowledge gathered from literature confirm that source of fluoride, carbon, and nitrogen species lies in electrolyte used in NTs preparation. Level of contamination depends on porosity and thickness of the films used in experiment, as well as composition of electrolyte and time of the anodization. However, it was confirmed by D. Regonini et al. that these species do not influence the degradation process [40,41]. They are common contaminants of TiO_2 nanotubes obtained by anodic oxidation, and all derive from the electrolyte [40,42].

The chemical character of Ti originating from pristine TiO_2 and Cu from the Cu-modified TiO_2 NTs were identified from the Ti 2p and Cu 2p HR XPS spectra, respectively. The selected spectra for 30 V are summarized in Table 2 and shown in Figure 3. The Ti 2p spectrum is resolved into two doublet-components at BE of Ti $2p_{3/2}$ signal at 458.7 and 457.3 eV and are assigned to Ti^{4+} and Ti^{3+}, respectively (Figure 3a). The Ti^{4+} is the dominant surface state and relative contribution of the Ti^{3+} species is similar for all NTs (Table 2). Following the curve-fitting procedure of Cu $2p_{3/2}$ spectra (Figure 3b), we separated the XPS peaks at the BE of 932.1 and 933.8 eV, which are characteristic of Cu(I) and Cu(II) oxide species, respectively [27,40,43–45]. The Cu(I) composites are the dominant Cu fraction for all samples, and their relative contribution depends on applied voltage during anodization process and amount of Cu in the Ti-Cu alloys (Table 2).

Inspection of the data presented in Table 2 reveal the relative contribution of Cu(I) fraction to be systematically increased as the Cu amount in the Ti-Cu alloys increased (see the XPS data for TiCu alloys anodized at 30 V).

Table 2. Surface properties and photoactivity of TiO_2/Cu_xO_y NTs and reference samples (pristine TiO_2 NTs).

Sample Label	Average Crystallite Size (nm)	XPS Analysis						Photocatalytic Reaction Rate, r (μmol·dm^{-3}·min^{-1})	
		∑ Ti (at.%)	Ti^{4+} 458.7 eV (%)	Ti^{3+} 457.3 eV (%)	Cu (at.%)	Cu^{1+} 932.2 eV (%)	Cu^{2+} 933.8 eV (%)	UV-Vis Light (λ > 350 nm)	Vis Light (λ > 420 nm)
Ti_30V	33	16.20	98.42	1.58	0	-	-	1.25	0.04
Ti_40V	27	24.79	97.38	2.62	0	-	-	1.35	0.13
Ti_50V	36	26.29	97.38	2.62	0	-	-	1.44	0.15
$Ti_{95}Cu_5$_30V	25	21.79	95.89	4.11	0.13	81.27	18.73	1.02	0.41
$Ti_{90}Cu_{10}$_30V	36	25.32	97.49	2.51	0.11	88.38	11.62	1.16	0.51
$Ti_{85}Cu_{15}$_30V	39	23.99	97.30	2.70	0.14	93.28	6.72	0.81	0.55
$Ti_{90}Cu_{10}$_40V	46	25.41	98.07	1.93	0.11	76.61	23.39	1.62	0.37
$Ti_{90}Cu_{10}$_50V	46	25.06	97.16	2.84	0.08	95.78	4.22	3.31	0.32

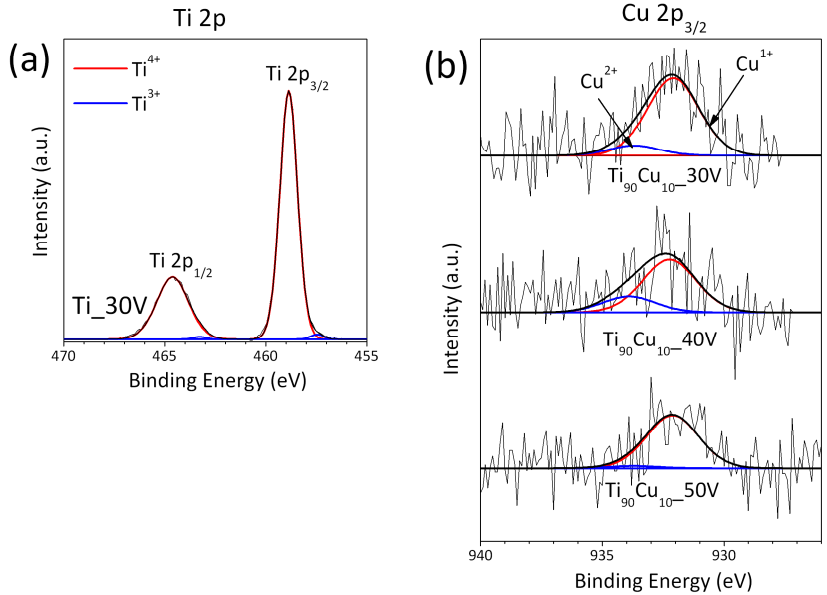

Figure 3. (**a**) Ti 2p XPS spectrum from the surface of pristine TiO_2 NTs (Ti_30V) and (**b**) Cu $2p_{3/2}$ XPS spectra of selected TiO_2/Cu_xO_y NTs ($Ti_{90}Cu_{10}$ alloys anodized at 30–50 V).

2.4. UV-Vis Spectra and Photoluminescence Properties

Figure 4a demonstrates UV-Vis spectra that were prepared for all investigated samples, not only alloys but also pristine NTs. The analysis results indicate clearly UV signals at the region 300–390 nm, which are strictly connected with the excitation state of the electrons and the movement from valence to conduction band [17]. $Ti_{95}Cu_5$_30V reflects high absorbance of UV light (λ < 380 nm) in comparison to pristine NTs. All modified NTs generally present more intensive absorbance in Vis irradiation range than pristine NTs, which can lead to intensified response during experiments in visible light. Maximum absorbance was observed at 600 nm with $Ti_{90}Cu_{10}$_30V, $Ti_{95}Cu_5$_30V, and $Ti_{85}Cu_{15}$_30V, and stands for red shift compared to pristine NTs. For $Ti_{90}Cu_{10}$_40V alloy, the absorbance maximum was not registered. Increased absorption values in Vis range in comparison to pristine NTs is a result of Cu_xO_y appearance in the system and their narrower band gap (Cu_2O = 2.1 eV; CuO = 1.7 eV), which work as a photo sensitizer that broadens the photo response of TiO_2 NTs to the visible region. The wide absorption band could have occurred because of inter-band transition in the Ti_xCu_y alloys. Figure 4a reveals a slight shift in band-gap transition of modified NTs to longer wavelengths. This effect can be assigned to stronger stabilization of the conduction band of TiO_2, Cu_2O, and CuO than their valence band [17].

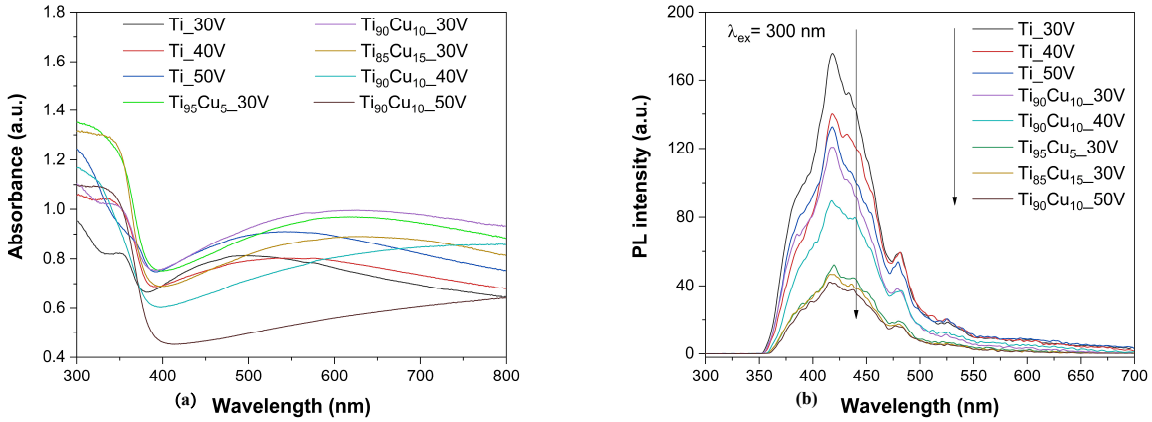

Figure 4. Absorbance (**a**) and photoluminescence (**b**) spectra of pristine TiO_2 and TiO_2/Cu_xO_y NTs.

The photoluminescence (PL) is a nondestructive spectroscopic technique often applied in study of intrinsic and extrinsic properties of both bulk semiconductors and nanostructures [46]. Mainly, the analysis of spectra of nanostructures can help in the characterization of the structure, providing information on the interface morphology and the quality of the materials. Photoluminescence (PL) signals and their intensity are closely related to photocatalytic activity. Possibly, the lower the PL intensity, the higher the separation rate of photo-induced charges, and, possibly, the higher the photocatalytic activity [47]. There are three intensive bands presented in Figure 4b, which can be distinguished. Two of them lie in the range between 400 and 440 nm and originate from charge recombination in the surface state defects [48]. The bands at 445–500 nm are attributed to different intrinsic defects in the TiO_2 lattice such as oxygen vacancies, titanium vacancies, and interstitial defects [49]. Because of different thicknesses of obtained NTs, the recombination rate intensity may be highly influenced. Figure 4b reveals TiO_2-Cu_xO_y NTs and pristine TiO_2 NTs response on PL, showing that TiO_2-Cu_xO_y NTs were more efficient than pristine TiO_2 NTs because of better charge carriers separation ability, which leads to improved photocatalytic properties.

2.5. Photodegradation Ability in Aqueous Phase

Photodegradation ability of obtained NTs was studied in phenol degradation process proceed in two different light sources: UV-Vis (λ > 350 nm) and Vis (λ > 420 nm) conditions. At the beginning,

a direct photolysis was performed to confirm the necessity of photocatalyst appearance. In case of UV-Vis irradiation, 3% of phenol was degraded, and in Vis light no action was observed. The significant results for UV-Vis were presented by samples with applied voltage above 30 V. $Ti_{90}Cu_{10}$_50V and $Ti_{90}Cu_{10}$_40V have degradation efficiencies close to 85% and 45%, respectively, while pristine NTs showed efficiency between 35–40% (Figure 5a). NTs obtained with voltage equal to 30 V revealed the efficiency lower than pristine NTs under UV-Vis light. The reason of obtained results is strictly connected with length of the NTs, as pristine NTs are longer (1.5–6 µm) than NTs from copper alloys anodized in 30 V, while in terms of $Ti_{90}Cu_{10}$_40V and $Ti_{90}Cu_{10}$_50V, NTs are just a little shorter (2.5–3.5 µm) than pristine NTs but sufficient for conducting the degradation process. Combination of length and Cu_2O and CuO species in total gives higher activity compering to pristine NTs. In terms of Vis light irradiation (Figure 5b), whose results were the main area of interest, the outcome appears to be different. The efficiency increased in the following order: Ti_30V < Ti_40V < Ti_50V < $Ti_{90}Cu_{10}$_50V < $Ti_{90}Cu_{10}$_40V < $Ti_{95}Cu_5$_30V < $Ti_{90}Cu_{10}$_30V < $Ti_{85}Cu_{15}$_30V showing that NTs obtained with 30 V presents the best results, reaching a value of 16% for the $Ti_{85}Cu_{15}$_30V sample. Obtained result can relate to the correlance of penetration depth of visible light and thickness of the NTs, in which only small amounts of photons can reach lower parts of the NTs. The level of influence on phenol degradation in terms of Vis light can lay also in amount of Cu in the sample. EDX results presented in Table 1 show that in $Ti_{85}Cu_{15}$_30V the highest amount of Cu was measured with the value of 9.45 (wt.%). The same results were obtained by XPS measurements (Table 2). Similar effect was observed during our previous work with the NTs obtained by anodic oxidation of Ti-Ag alloys [50].

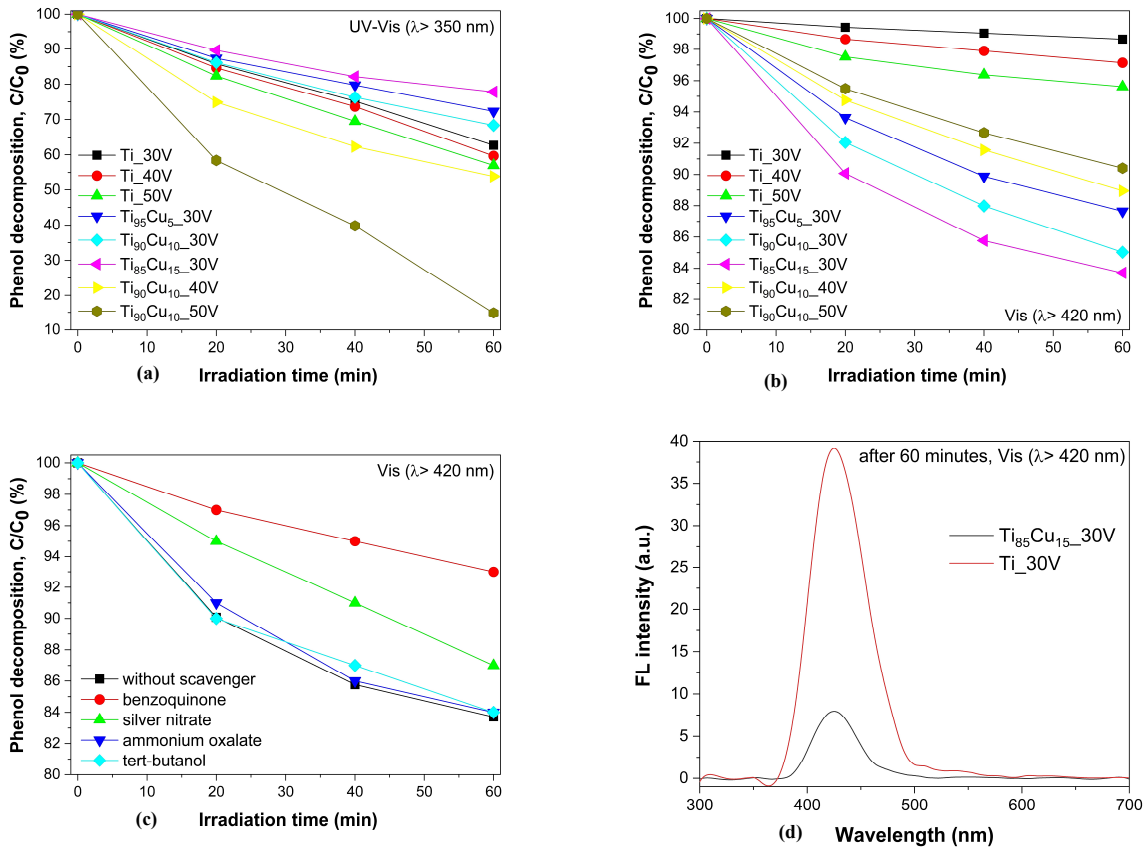

Figure 5. Kinetics of photocatalytic degradation of phenol under UV-Vis (**a**) and Vis (**b**) irradiation, photocatalytic decomposition of phenol under visible light irradiation in the presence of scavengers, and $Ti_{95}Cu_{15}$_30V sample (**c**) and •OH radical generation efficiency under Vis irradiation (**d**) in the presence of selected samples.

2.6. The Excitation Mechanism of TiO_2-Cu_xO_y NTs

For better understanding of the visible light excitation mechanism of TiO_2, NTs modified with Cu species additional experiments were performed. First of all, to confirm phenol degradation mechanism, reactions with different scavengers-benzoquinone (for $O_2\bullet^-$ radicals), silver nitrate (for e^-), ammonium oxalate (for h^+), and tert-butanol (for hydroxyl radicals) were performed for the most active sample $Ti_{85}Cu_{15}$_30V, as shown in Figure 5c. The photocatalytic efficiency of phenol degradation for benzoquinone was 13% and for silver nitrate 6%. In terms of other scavengers, the degradation was negligible in comparison with the reaction without scavengers what can lead to conclusions that $O_2\bullet^-$ radicals are the main initiator of photocatalytic degradation under visible light irradiation. Secondly, to confirm above results, the •OH radical generation tests were taken (see Figure 5d), confirming that larger amounts of •OH radicals were produced in case of pristine NTs than in presence of TiO_2-Cu_xO_y NTs. It can incline that other forms of reactive oxygen species are the source of phenol degradation under Vis light (as demonstrated in Figure 6a).

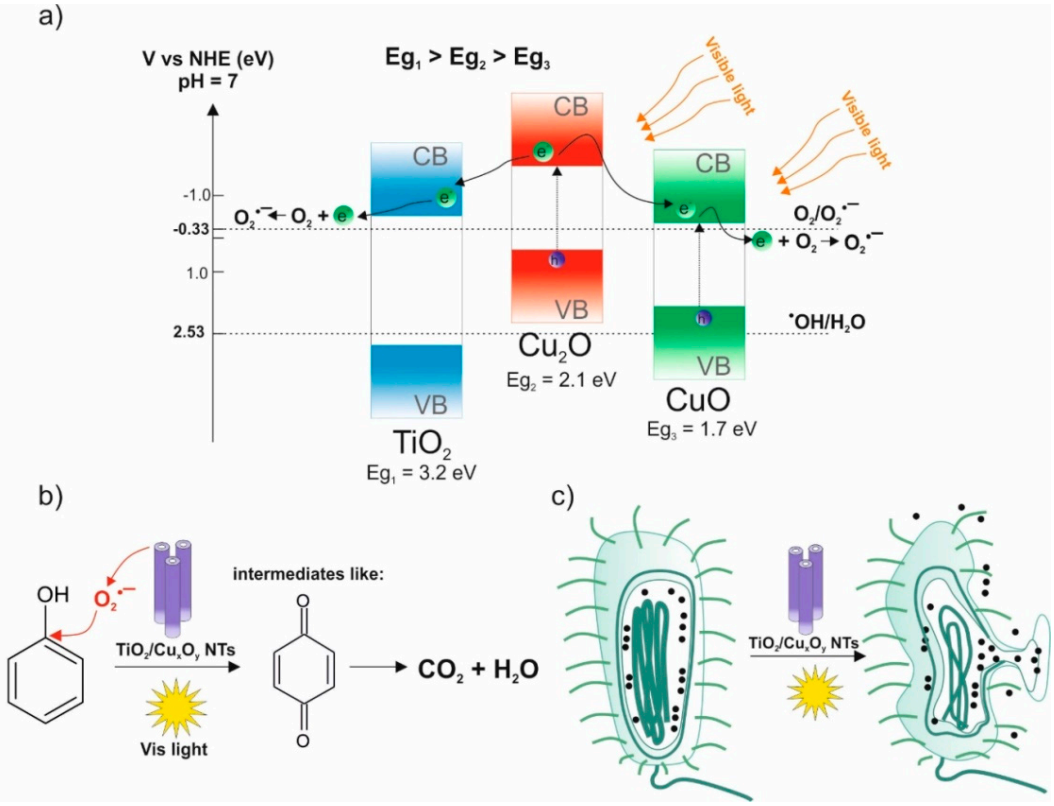

Figure 6. A suggested scheme of (**a**) visible light excitation mechanism in presence of TiO_2-Cu_2O and CuO NTs, (**b**) phenol degradation pathway under Vis light, and (**c**) inactivation of bacterial cell by $O_2\bullet^-$ radicals.

As the results of XPS showed division of the TiO_2-Cu_xO_y NTs in terms of Cu type, the Vis light photocatalytic mechanism (Figure 6a) and the stability of heterojunctions should be considered for both types Cu^+ and Cu^{2+}. As the TiO_2 NTs band gap (3.2 eV) is too wide to absorb Vis light, TiO_2-Cu_2O were investigated for band gaps much narrower 2.1 eV and 1.7 eV, respectively, to confirm the application of materials in Vis light. TiO_2-Cu_2O and TiO_2-CuO NTs with the Vis light conditions can activate electrons and create the pair electron-hole [51]. In terms of TiO_2-Cu_2O NTs, electron from CB Cu_2O is transferred to the conduction band of TiO_2 NTs, whereas holes from valence band of Cu_2O remain immobile and are unable to generate •OH radicals, because the band edge potential is lower than edge for •OH radical generation with potential of 2.53 eV. The electron path from CB of TiO_2 NTs

transfers further to the environment reacting with the oxygen and creating superoxide anion radicals $O_2\bullet^-$ and then H_2O_2 and $HO_2\bullet$. When analyzing the reaction with TiO_2-CuO NTs, the situation is very much different. As the band gap of CuO (1.7 eV) enables electrons to move conduction band of CuO, the electrons react with oxygen forming superoxide anion radicals $O_2\bullet^-$ and then H_2O_2 and $HO_2\bullet$. Furthermore, the reaction with pollutant (phenol) after several processes led to formation of intermediates and finally H_2O and CO_2 (as shown in Figure 6b).

Moreover, it is confirmed that redox potentials for the reduction of Cu_2O to Cu and for oxidation Cu_2O to CuO occur and should be taken into consideration. However, Weng et al reported that in presence of even small amount of CuO, which works as a protection shield, the possibility of Cu_2O photocorrosion is less probable [52]. XPS analysis showed (Table 2) that there are trace amounts of CuO in tested NTs alloys that can lead to the conclusion that Cu_2O is resistant to photocorrosion process. All results above and analysis presented by Luna et al. [53] can lead to proposed Cu_2O-CuO-TiO_2 complex mechanism (Figure 6a).

2.7. Assessment of Antibacterial Properties of TiO_2/Cu_xO_y NTs

Microbial contamination of the environment can be a critical issue for many aspects of our lives. That is why the modification of surface with different additives, which can foster the process of bacterial inactivation, is important [54]. The assessment of the antibacterial properties of photocatalytic layer—TiO_2/Cu_xO_y NTs obtained from $Ti_{95}Cu_5$ alloy in Vis light—was investigated in three different configurations in presence of microorganisms, Ti-Cu NTs, Vis light, microorganisms and Vis light only, and microorganisms and Ti-Cu NTs in the dark. Three different bacterial strain were used: *E. coli*, *B. subtilis*, and *Clostridium* sp. The amount of bacteria after the process was measured quantitatively (CFU/mL (colony-forming unit)) and with usage of TEM (Table 3 and Figure 7, respectively).

Table 3. Efficiency of bacteria inactivation in aqueous phase in the presence of the $Ti_{95}Cu_5$_30V sample and visible light (λ > 420 nm).

Bacterial Strain	Experimental Conditions	Efficiency after 60 min
***E. coli* — OD = 0.09** **STARTING CFU/mL: 3.3 × 10^2**	Light source: switched on Bacteria: present Photocatalytic layer: present	97%
	Light source: switched off Bacteria: present Photocatalytic layer: present	12%
	Light source: switched on Bacteria: present Photocatalytic layer: absent	3%
***B. subtilis* — OD = 0.09** **STARTING CFU/mL: 2.5 × 10^2**	Light source: switched on Bacteria: present	Did not grow
	Photocatalytic layer: present Light source: switched off Bacteria: present Photocatalytic layer: present	Did not grow
	Light source: switched on Bacteria: present Photocatalytic layer: absent	16%
***Clostridium* sp. — OD = 0.1** **STARTING CFU/mL: 3.8 × 10^2**	Light source: switched on Bacteria: present Photocatalytic layer: present	98%
	Light source: switched off Bacteria: present Photocatalytic layer: present	0%
	Light source: switched on Bacteria: present Photocatalytic layer: absent	5%

The quantitative analysis shows that correlation between efficiency of the process and experimental conditions are clearly noticeable. The significant results were obtained for measurements in presence of Vis light source and photocatalytic layers in case of two strains: *E. coli* (97% damage in 60 min) and *Clostridium* sp. (98% damage in 60 min). What is more, in example of *B. subtilis* there was no response of bacteria and it never grew (all results presented in Table S3). The lack of *B. subtilis* growth can be related to conditions of the experiment or the influence of Cu^{2+} ions leached from surface of nanotubes.

B. subtilis can form endospores which are small, metabolically dormant cells remarkably resistant to heat, desiccation, radiation, and chemical insult. Sporulation is the last response to nutrient starvation or other stressful conditions. Alternative condition to forming the spores is high cell density favors sporulation. The process of endospore formation has profound morphological and physiological consequences [55,56]. Endospores are produced in a process called sporulation, which is reversible, because the vegetative cell can be regenerated again when only in the environment there will be favorable conditions. This reverse process to sporulation is called germination of spores. This process requires a number of spore specific proteins. Most proteins are associated with the inner spore membrane [57]. Germination of spores depends on many conditions present in bacterial growth and formulation way of spores. Stress conditions for bacteria (irradiation of the catalytic layer connected radiation) led to the formation of spores, which under normal conditions of Bacillus sp. growth were unable to undergo germination.

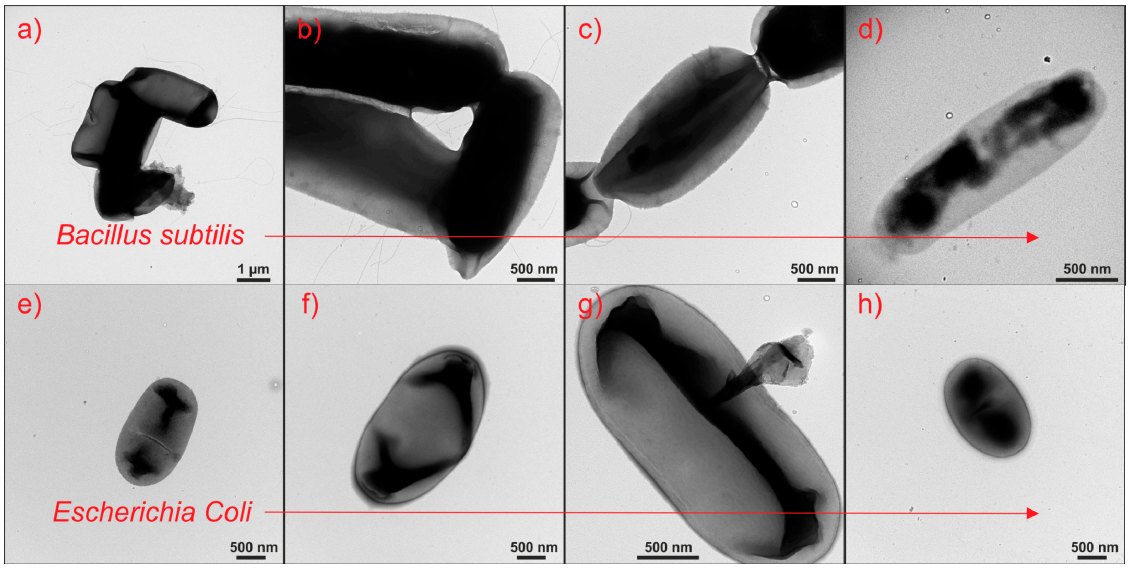

Figure 7. TEM images of bacteria after 60 min of various processes: (**a**,**e**) reference bacteria (**b**,**f**) light switched off, bacteria present, photocatalyst present, (**c**,**g**) light switched on, bacteria present, photocatalyst absent and (**d**,**h**) light switched on, bacteria present, photocatalyst present.

However, there are also differences between germination of *Bacillus spores* and *Clostridium spores*. First, while germinant receptor (GR) function in germination *Bacillus* sp. requires all three GR subunits. It appears that only a GRc subunit alone can facilitate *Clostridia spore* germination. Second, spores of some *Clostridia* lack GRs with any similarity to those in spores of bacilli, likely a reflection of the great diversity in the *Clostridia*. However, *C. difficile spores* do germinate well with specific bile salts and also respond to various amino acids [57]. In the case of *E. coli*, these types of processes are not observed because they do not sporulate.

For confirmation of previous analysis, the effect of Cu^{2+} on the growth of *E. coli* and *B. subtilis* was investigated (Figure S3 and Table S4). The growth of bacterial cultures (with the addition of Cu^{2+} ions) was controlled by measuring the optical density at 600 nm. Growth inhibition was found for

both strains in the first two dilutions. The minimal inhibitory concentration (MIC) is 0.1 mM of Cu^{2+} ions. A similar effect was observed by Zong et al. [34]. After obtaining above results, only *E. coli* and *B. subtilis* were sent for TEM analysis to confirm the transformation of bacteria. Images revealed changes in bacteria shape in every tested configuration with the biggest influence of photocatalytic layer on *B. subtilis* (clear damage of the inside structure) and light source on *E. coli* (whole deformation of bacteria). Deformed bacterial cell cannot grow and is no longer a serious environmental problem. Finally, it is likely that the cell membrane will undergo complete mineralization [58]. In summary, the as-prepared photocatalyst irradiated with Vis light has very high, indisputable bactericidal effects (in both cases, efficiency of bacteria inactivation reached 97%). *E. coli*, *Clostridium* sp., and *B. subtilis* are removed from water and the surface of the photocatalysts within 60 min. of irradiation.

2.8. Suggested Mechanism of Bacteria Inactivation

A full knowledge about the mechanism of bacteria inactivation is essential for further development of nanocomposites involved in disinfection processes. Matsunga et al. were the pioneers with hypothesis in which Coenzyme A is degraded by ROS in the presence of light [21]. The enzyme cut off can cause respiration problems, possibly leading to death. However further research performed by Saito et al. confirmed that main reason for cell death is the burst of the cell wall membrane leading to leakages [59]. Obtained TEM images (Figure 7) for experiment with $Ti_{95}Cu_5$_30V confirmed the destruction of bacteria cell structure and wall membrane in presence of photocatalyst and light, which led to conclusion that copper as a component photocatalyst influenced the process. Moreover, based on analysis made by Kikuchi et al., who confirmed the role of the ROS by addition of hydroxyl scavengers to the reaction system [60], it can be concluded that for TiO_2-Cu_XO_y, another source of bacteria inactivation lies in oxygen radicals. The suggested scheme presenting damage of bacteria cell during the inactivation process is presented in Figure 6c.

3. Materials and Methods

3.1. Materials

The titanium foils and alloys were purchased from HMW Hauner (Röttenbach, Germany). Isopropanol, acetone, and methanol (p.a., POCh S.A., Gliwice, Poland) were used for cleaning Ti foil and alloys surface. NH_4F (p.a.) and ethylene glycol (99.0%, p.a.) purchased from POCh S.A. were the components of the electrolyte, which were used for preparation of the TiO_2 nanotubes. Deionized water used during experiments had conductivity of 0.05 μS.

The following bacterial strains were used in this work: *E. coli* DSMZ collection no 1116, *B. subtilis* DSMZ collection no 347, and *Clostridium* sp. DSMZ collection no 2634. *E. coli* is a Gram-negative, facultatively anaerobic, rod-shaped bacteria. *E. coli* is found in the gut of animals, including human gut, as well as commonly in soil and water. Bacteria does not create endospores. *B. subtilis* is Gram-positive, facultative anaerobe, and rod-shaped found in soil and the gastrointestinal tract of ruminants and humans. It can form a tough, protective endospore, allowing it to tolerate extreme environmental conditions. *Clostridium* sp. is Gram-positive, obligate anaerobes, rod-shaped bacteria. They are producing endospores commonly found mainly in the soil and digestive tract of animals, including humans, female reproductive organs, as well as in water and sewage. These bacteria are characterized by the possibility of binding atmospheric nitrogen and reduction of sulphites [61].

To measure the copper influence on growth of bacteria cultures, the bacterial cultures mentioned above were conducted in LB medium (1% tryptone, 0.5% yeast extract, 1% NaCl, pH 7.0), supplemented with 98% copper acetate ($C_4H_6CuO_4 \times H_2O$) from Avantor Performance Materials S.A. (Gliwice, Poland).

3.2. Preparation of NTs

Ti and Ti-Cu alloys containing different amounts of copper (5, 10, 15 wt.%) in the form of sheets were cut into pieces of size 2 × 3 cm. In the first step, experiment samples were cleaned with usage of acetone, isopropanol, methanol, and deionized water separately, one by one, in ultrasonic bath for 10 min. Cleaning process was finalized with drying alloys in the air steam. In the second step, the set up for anodization process was established with two electrodes-platinum mesh as the cathode and Ti/Ti-Cu alloy as a working electrode. Moreover, the Ag/AgCl reference electrode was incorporated into the system to gather information about the definite potential of the electrode. The anodic oxidation process was performed in the presence of electrolyte solution (98 vol % ethylene glycol, 2 vol % water and 0.09 M NH_4F) for 60 min with applied voltage in a range between 30 and 50 V. The anodization was monitored with DC power supply (MANSON SDP 2603, Hong Kong, China). After all, in third step, samples were sonicated in deionized water for 5 min, dried in air stream at 80 °C for 24 h, and calcinated at 450 °C (heating rate of 2 °C/min) for 1 h.

3.3. Characterization Systems

To understand the morphology of NTs obtained by electrochemical method, scanning electron microscopy was performed (SEM-FEI Quanta 250 FEG FEI Company, Brno, Czech Republic). To locate the anomalies, structure high-resolution transmission electron microscopy (HRTEM Jeol ARM 200F, Akishama, Tokio, Japan)) was carried out. The X-Ray photoelectron spectroscopy (XPS) measurements were completed at PHI 5000 VersaProbeTM (ULVAC-PHI, Chigasaki, Japan) spectrometer with monochromatic Al Kλ radiation (hν = 1486.6 eV). Phase composition on the surface was checked using a room temperature powder X-ray X'Pert Pro MPD diffractometer (PANalytical, Almelo, The Netherlands)(CuKαλ 1.5406 Å). A LeBail refinement was performed using the HighScore software (Ver. 3.0d, PANanalytical, Almelo, The Netherlands). The binding energy (BE) scale of all detected high resolution (HR) spectra was referenced by setting the BE of the aliphatic carbon peak (C-C) signal to 284.6 eV. The photoluminescence (PL) measurements were taken at room temperature with LS-50B Luminescence Spectrophotometer with Xenon discharge lamp as an excitation source and special detector—a R928 photomultiplier (HAMAMATSU, Hamamatsu, Japan). The excitation radiation (360 nm) was directed on the sample's surface at an angle of 90°. The UV-Vis reflectance and absorbance spectra of pure and copper doped NTs were obtained with usage of Shimadzu UV-Vis. Spectrophotometer (UV 2600) (SHIMADZU, Kioto, Japan), with reference samples of barium sulphate. The range for the spectra registration was between 300 and 800 nm in room temperature and set scanning speed of 250 nm/min.

3.4. Photocatalytic Activity

The equipment used for all photocatalytic activity measurements was as follows: a quartz reactor with the capacity of 10 mL, 1000 W Xenon Lamp (Oriel 66021 Stratford, CT, USA), and cut off filters. Light intensity was measured for both filters with value of 40 mW/cm^2 for UV-Vis and 2 mW/cm^2 for Vis range.

3.4.1. Phenol Degradation Process

The process of photocatalytic degradation in model reaction with usage of phenol for two light sources was performed. The irradiation was controlled by two cut off filters GG350 (UV-Vis λ > 350 nm) and GG 420 (Vis λ > 420 nm). To perform the experiment, prepared phenol solution (20 mg/L) in amount of 8 mL was applied to the reactor, followed by immersing the examined alloy. Prepared sample was placed on a stirrer (500 rpm) and irradiated with preferable light for 60 min. Not only reference phenol solution (0.5 mL) was taken before the beginning of procedure, but also samples (0.5 mL) after each 20 min of the irradiated process were collected. We chose colorimetric method in the

presence of p-nitroaniline and with usage of UV-Vis spectrophotometer (λ_{max} = 480 nm) to investigate the phenol concentration.

3.4.2. Microorganisms Inactivation Process

The experiment connected with bacteria inactivation process was performed with application of three microorganisms species—*E. coli*, *B. subtilis*, and *Clostridium* sp. All vessels and media used in bacterial experiments were pre-sterilized by steam. The preparation of bacteria were harvested in LB medium by shaken in air shaker at 37 °C for 16 h. The bacteria pellet was isolated from medium by centrifugation at 2739 × *g* for 10 min. The resulting pellet was resuspended in sterile water to final concentration *E. coli* 3.3×10^2, *B. subtilis* 2.5×10^2, *Clostridium* sp. 3.8×10^2 (OD_{600nm} = 0.1). As it is proven that microorganisms die in UV irradiation range, the Vis range with the cut off filter GG420 was used. As a photocatalyst, $Ti_{95}Cu_5$ alloy was applied.

The idea of the experiment was to check the inactivation process in three control tests—in presence of microorganisms, Ti-Cu NTs, and Vis light; in presence of microorganisms and Vis light only; and in the presence of microorganisms and Ti-Cu NTs in the dark. To perform the experiment, the suspension of bacteria (8 mL) was applied in the same reactor as in phenol degradation process. Depending on the configuration, Ti-Cu NTs were immersed in bacteria suspension or not. Prepared set up (with or without NTs) was placed on a stirrer (500 rpm) and irradiated with preferable light or kept in the dark for 60 min. Reference samples (1 mL) were collected just before each experiment, and consecutive samples (1 mL) were taken every 20 min. After the complete process there were two procedures of measurements. First, the collected samples were prepared by serial dilution (100 µL of sample in 900 µL of sterile 1 × PBS (phosphate-buffered saline)) and subsequent 10 µL of each were seeded on agar plate PCA (Plate Count Agar). The plates were incubated at 37 °C in an incubator for 16 h. Grown bacteria were counted, along with the amount of microorganisms in 1 mL of the dilution with the formula CFU = number of colonies × dilution/volume of inoculum. Second time, more diluted consecutive samples (1 mL taken every 20 min) were put in the ice and sent to resolution transmission electron microscopy.

3.4.3. Measurement of Copper Cu^{2+} Influence on Growth of Bacterial Cultures

The aim of the measurement was to check the influence of Cu^{2+} on the growth of bacterial cultures. This method was chosen to identify if the copper alone influenced the bacteria. The diluted solution of copper actetite was used to perform this measurement. The bacteria were harvested in LB medium by shaken in air shaker at 37 °C for 16 h. *B. subtilis* was added to LB medium to OD_{600nm} = 0.13 and *E. coli* to OD_{600nm} = 0.1 and were harvested in air shaker at 37 °C for 30 min. In the test tube, serial dilution of Cu^{2+} ions were prepared from 1–1×10^{-9} mM. Then, OD_{600nm} was measured; the negative control was LB medium, and the positive control was LB medium with bacteria with appropriate OD_{600nm}.

To determine the influence of Cu^{2+} ions on *B. subtilis* culture, the 2-fold serial dilution test of ions was tested. The *B. subtilis* was culture in LB medium by shaken in air shaker at 37 °C for 16 h. *B. subtilis* was added to LB medium to OD_{600nm} = 0.1 and harvested in air shaker at 37 °C for 1.5 h. In the test tube 2-fold serial dilution of Cu^{2+}, ions were prepared from 10–1.9×10^{-2}. The OD_{600nm} was measured every 30 min; the negative control was LB medium, and the positive control was LB medium with bacteria with appropriate OD_{600nm}.

3.4.4. Measurement of Hydroxyl Radicals

As •OH radicals are considered the most powerful in the oxidation process of many organic compounds [62], the role and amount was determined to understand the photocatalytic properties. A terephthalic acid, as a substance which effectively captures •OH radicals and generates highly fluorescent product, was used and investigated for photoluminescence intensity. The tests were performed in the same laboratorium set up as in the phenol degradation process with the initial concentration of terephthalic acid equal Co. = 0.5 mM. The reactor was irradiated for 60 min,

with 20 min intervals for sample collection. The photoluminescence spectra of all collected samples were measured at LS–50 B luminescence spectrophotometer (HAMAMATSU, Hamamatsu, Japan) with lamp with excitation wavelength at 315 nm and photomultiplier detector.

3.4.5. Investigation of Photodegradation Mechanism

In order to understand the mechanism of photodegradation of phenol solution silver nitrate, ammonium oxalate, tert-buthyl alcohol, and benzoquinone were applied, which are scavengers for e^-, h^+, •OH, and $O_2\bullet^-$ radicals, respectively. The photodegradation experiment conditions were the same as in phenol degradation process.

4. Conclusions

The analysis of new spectra of nanostructures developed by electrochemical method TiO_2/Cu_xO_y NT arrays due to their unique features can be used not only in the photodegradation process but also in bacteria inactivation. In this study, the influence of copper amount and applied voltage in NTs formation was investigated, as well as the correlation of NTs composition with the efficiency of the photodegradation of pollutants in the aqueous phase. All prepared Ti_xCu_y foils after the anodization process have proved to be self-organized nanotubes arrays with external diameter of 85–97 nm and length 1.1–3.5 μm. The dimensions were directly induced by applied voltage, as the NTs were usually shorter and thicker than pristine TiO_2 NTs. Furthermore, photodegradation of phenol in the aqueous phase with the presence of NT photocatalysts was performed under Vis light irradiation ($\lambda > 420$ nm). The best performance was marked in the case of TiO_2/Cu_xO_y NTs arrays with a Cu content of 15 wt.%. Additionally, PL analysis and absorbance measurements were performed that revealed promising results in terms of NTs application in Vis light region. It was proved that oxygen vacancies activated by Cu dopant in the NTs could be the main factor in the phase stabilization of the anataze phase.

Moreover, the assessment of the antibacterial properties of new NTs was performed with very promising results regarding the efficiency of bacteria degradation in terms of *E. coli* (97% degradation in 60 min) and *Clostridium* sp. (98% degradation in 60 min) under visible light irradiation (using low CFU/mL of bacteria).

The anodization method with Cu-Ti alloys developed in this study is a simple and effective method that can be implemented on a larger scale, not only in environmental applications but also in medical industry. Our results are encouraging and should be continued in the study of complexes with more than two components during anodization. Further work needs to be carried out in direction of creating nanomaterials with cascade heterojunctions possessing accurate photoelectrochemical characterization, which can be cheaper and more controlled in comparison to two composite photocatalysts. Research in this area was already undertaken by analyzing Cu-Ag-Ti alloys. It is also a challenge to consider the antibiotic resistant strains of mutant microbs, which are a growing problem nowadays. Finally, what seems to be an important matter is the variety of standards used by research group to measure the efficiency of the photocatalysts and their influence on microorganisms.

Supplementary Materials: The following are available online at http://www.mdpi.com/2073-4344/8/6/237/s1, Figure S1: Top-view and cross-sectional SEM images of pristine TiO_2 NTs, Figure S2: X-ray diffraction patterns for pristine TiO_2 NTs, Table S1: Refined lattice parameters for TiO_2—anatase, Ti—metal and $CuTiO_2$—alloy. The crystallite size was calculated for the anatase only, Table S2: Elemental composition (in at.%) in the surface layer of TiO_2 and Cu-modified TiO_2 NTs, evaluated by XPS analysis, Table S3: Efficiency of bacteria inactivation after 20, 40 and 60 min of various processes, Figure S3: Image of influence of Cu^{2+} ions on the growth of *B.Subtilis*, Table S4: The influence of Cu^{2+} ions on the growth of *E. coli* and *B. subtilis*. (a) OD measurements at 600 nm of *E. coli* and *B. subtilis* cultures with the addition of Cu^{2+} ions from 1–1 $\times$ 10^{-9} mM (serial dilution), (b) OD measurements at 600 nm of *B. subtilis* culture with addition of Cu^{2+} ions from 10–1.9 $\times$ 10^{-2} from 1–10^{-9} mM. To, T1, T2—the subsequent measurement points; Kp—positive control, culture of strain without Cu^{2+} ions; Kn—negative control, the medium.

Author Contributions: Conceptualization: A.Z.-M. and P.M.; methodology: A.Z.-M. and P.M.; investigation: M.K. (Magda Kozak), P.M., J.Ż., M.K. (Marek Kobylański), T.K., W.L., G.T., and G.N.; visualization: M.K. (Magda Kozak)

and P.M.; writing-original draft preparation: M.K. (Magda Kozak) ; writing review & reediting: P.M and A.Z.-M.; supervision: A.Z.-M.; funding acquisition: A.Z.-M.

Funding: This research was financially supported by the Polish National Science Center (grant No. NCN 2014/15/B/ST5/00098, ordered TiO_2/M_xO_y nanostructures obtained by electrochemical method).

Conflicts of Interest: The authors declare no conflict of interest.

References

1. Hoffmann, M.R.; Martin, S.T.; Choi, W.; Bahnemann, D.W. Environmental Applications of Semiconductor Photocatalysis. *Chem. Rev.* **1995**, *95*, 69–96. [CrossRef]
2. Fujishima, A.; Rao, T.N.; Tryk, D.A. Titanium dioxide photocatalysis. *J. Photochem. Photobiol. C Photochem. Rev.* **2000**, *1*, 1–21. [CrossRef]
3. Low, J.; Cheng, B.; Yu, J. Surface modification and enhanced photocatalytic CO_2 reduction performance of TiO_2: A review. *Appl. Surf. Sci.* **2017**, *392*, 658–686. [CrossRef]
4. Ni, M.; Leung, M.K.H.; Leung, D.Y.C.; Sumathy, K. A review and recent developments in photocatalytic water-splitting using TiO_2 for hydrogen production. *Renew. Sustain. Energy Rev.* **2007**, *11*, 401–425. [CrossRef]
5. Yadav, H.M.; Kim, J.-S.; Pawar, S.H. Developments in photocatalytic antibacterial activity of nano TiO_2: A review. *Korean J. Chem. Eng.* **2016**, *33*, 1989–1998. [CrossRef]
6. Zhang, S.; Zhang, S.; Peng, F.; Zhang, H.; Liu, H.; Zhao, H. Electrodeposition of polyhedral Cu_2O on TiO_2 nanotube arrays for enhancing visible light photocatalytic performance. *Electrochem. Commun.* **2011**, *13*, 861–864. [CrossRef]
7. Pelaez, M.; Nolan, N.T.; Pillai, S.C.; Seery, M.K.; Falaras, P.; Kontos, A.G.; Dunlop, P.S.M.; Hamilton, J.W.J.; Byrne, J.A.; O'Shea, K.; et al. A review on the visible light active titanium dioxide photocatalysts for environmental applications. *Appl. Catal. B Environ.* **2012**, *125*, 331–349. [CrossRef]
8. Nevárez-Martínez, M.; Kobylański, M.; Mazierski, P.; Wółkiewicz, J.; Trykowski, G.; Malankowska, A.; Kozak, M.; Espinoza-Montero, P.; Zaleska-Medynska, A. Self-Organized TiO_2–MnO_2 Nanotube Arrays for Efficient Photocatalytic Degradation of Toluene. *Molecules* **2017**, *22*, 564. [CrossRef]
9. Daraio, C.; Jin, S. Synthesis and Patterning Methods for Nanostructures Useful for Biological Applications. In *Nanotechnology for Biology and Medicine*; Silva, G.A., Parpura, V., Eds.; Springer: New York, NY, USA, 2012; pp. 27–44. ISBN 978-0-387-31282-8.
10. Nevárez-Martínez, M.; Mazierski, P.; Kobylański, M.; Szczepańska, G.; Trykowski, G.; Malankowska, A.; Kozak, M.; Espinoza-Montero, P.; Zaleska-Medynska, A. Growth, Structure, and Photocatalytic Properties of Hierarchical V_2O_5–TiO_2 Nanotube Arrays Obtained from the One-step Anodic Oxidation of Ti–V Alloys. *Molecules* **2017**, *22*, 580. [CrossRef]
11. Mohammed, M.T.; Khan, Z.A.; Siddiquee, A.N. Surface Modifications of Titanium Materials for developing Corrosion Behavior in Human Body Environment: A Review. *Procedia Mater. Sci.* **2014**, *6*, 1610–1618. [CrossRef]
12. Jung, M.; Scott, J.; Ng, Y.H.; Jiang, Y.; Amal, R. CuO x dispersion and reducibility on TiO_2 and its impact on photocatalytic hydrogen evolution. *Int. J. Hydrogen Energy* **2014**, *39*, 12499–12506. [CrossRef]
13. Gong, D.; Grimes, C.A.; Varghese, O.K.; Hu, W.; Singh, R.S.; Chen, Z.; Dickey, E.C. Titanium oxide nanotube arrays prepared by anodic oxidation. *J. Mater. Res.* **2001**, *16*, 3331–3334. [CrossRef]
14. Macak, J.M.; Schmuki, P. Anodic growth of self-organized anodic TiO_2 nanotubes in viscous electrolytes. *Electrochim. Acta* **2006**, *52*, 1258–1264. [CrossRef]
15. Xie, Z.B.; Blackwood, D.J. Effects of anodization parameters on the formation of titania nanotubes in ethylene glycol. *Electrochim. Acta* **2010**, *56*, 905–912. [CrossRef]
16. Erjavec, B.; Tišler, T.; Tchernychova, E.; Plahuta, M.; Pintar, A. Self-Doped Cu-Deposited Titania Nanotubes as Efficient Visible Light Photocatalyst. *Catal. Lett.* **2017**, *147*, 1686–1695. [CrossRef]
17. Hai, Z.; EL Kolli, N.; Chen, J.; Remita, H. Radiolytic synthesis of Au–Cu bimetallic nanoparticles supported on TiO_2: Application in photocatalysis. *New J. Chem.* **2014**, *38*, 5279–5286. [CrossRef]
18. Lalitha, K.; Sadanandam, G.; Kumari, V.D.; Subrahmanyam, M.; Sreedhar, B.; Hebalkar, N.Y. Highly Stabilized and Finely Dispersed CuO/TiO: A Promising Visible Sensitive Photocatalyst for Continuous Production of Hydrogen from Glycerol:Water Mixtures. *J. Phys. Chem. C* **2010**, *114*, 22181–22189. [CrossRef]

19. Geng, Z.; Zhang, Y.; Yuan, X.; Huo, M.; Zhao, Y.; Lu, Y.; Qiu, Y. Incorporation of Cu_2O nanocrystals into TiO_2 photonic crystal for enhanced UV–visible light driven photocatalysis. *J. Alloys Compd.* **2015**, *644*, 734–741. [CrossRef]
20. Colón, G.; Maicu, M.; Hidalgo, M.C.; Navío, J.A. Cu-doped TiO_2 systems with improved photocatalytic activity. *Appl. Catal. B Environ.* **2006**, *67*, 41–51. [CrossRef]
21. Matsunaga, T.; Tomoda, R.; Nakajima, T.; Wake, H. Photoelectrochemical sterilization of microbial cells by semiconductor powders. *FEMS Microbiol. Lett.* **1985**, *29*, 211–214. [CrossRef]
22. *Polymeric Materials with Antimicrobial Activity: From Synthesis to Applications*; Muñoz-Bonilla, A.; Cerrada, M.; Fernández-García, M. (Eds.) Polymer Chemistry Series; Royal Society of Chemistry: Cambridge, UK, 2013; ISBN 978-1-84973-807-1.
23. Chen, L.; Luo, T.; Yang, S.; Xu, J.; Liu, Z.; Wu, F. Efficient metoprolol degradation by heterogeneous copper ferrite/sulfite reaction. *Environ. Chem. Lett.* **2018**, *16*, 599–603. [CrossRef]
24. Wojcieszak, D.; Mazur, M.; Kaczmarek, D.; Poniedziałek, A.; Osękowska, M. An impact of the copper additive on photocatalytic and bactericidal properties of TiO_2 thin films. *Mater. Sci. Pol.* **2017**, *35*. [CrossRef]
25. Reilche, H.; Dunn, W.W.; Bard, J.A. Allen Heterogeneous photocatalytic and photosynthetic deposition of copper on TiO_2 and WO_3 powders. *J. Phys. Chem.* **1979**, *83*, 2248–2251.
26. Moniz, S.J.A.; Tang, J. Charge Transfer and Photocatalytic Activity in CuO/TiO_2 Nanoparticle Heterojunctions Synthesised through a Rapid, One-Pot, Microwave Solvothermal Route. *ChemCatChem* **2015**, *7*, 1659–1667. [CrossRef]
27. Hu, Q.; Huang, J.; Li, G.; Chen, J.; Zhang, Z.; Deng, Z.; Jiang, Y.; Guo, W.; Cao, Y. Effective water splitting using CuO x/TiO_2 composite films: Role of Cu species and content in hydrogen generation. *Appl. Surf. Sci.* **2016**, *369*, 201–206. [CrossRef]
28. Ma, Q.; Liu, S.J.; Weng, L.Q.; Liu, Y.; Liu, B. Growth, structure and photocatalytic properties of hierarchical Cu–Ti–O nanotube arrays by anodization. *J. Alloys Compd.* **2010**, *501*, 333–338. [CrossRef]
29. Gao, L.; Qiu, Z.; Gan, W.; Zhan, X.; Li, J.; Qiang, T. Negative Oxygen Ions Production by Superamphiphobic and Antibacterial TiO_2/Cu_2O Composite Film Anchored on Wooden Substrates. *Sci. Rep.* **2016**, *6*. [CrossRef]
30. Cheng, M.; Yang, S.; Chen, R.; Zhu, X.; Liao, Q.; Huang, Y. Copper-decorated TiO_2 nanorod thin films in optofluidic planar reactors for efficient photocatalytic reduction of CO_2. *Int. J. Hydrogen Energy* **2017**, *42*, 9722–9732. [CrossRef]
31. He, X.; Zhang, G.; Wang, X.; Hang, R.; Huang, X.; Qin, L.; Tang, B.; Zhang, X. Biocompatibility, corrosion resistance and antibacterial activity of TiO_2/CuO coating on titanium. *Ceram. Int.* **2017**, *43*, 16185–16195. [CrossRef]
32. Yadav, H.M.; Otari, S.V.; Koli, V.B.; Mali, S.S.; Hong, C.K.; Pawar, S.H.; Delekar, S.D. Preparation and characterization of copper-doped anatase TiO_2 nanoparticles with visible light photocatalytic antibacterial activity. *J. Photochem. Photobiol. A Chem.* **2014**, *280*, 32–38. [CrossRef]
33. Nischk, M.; Mazierski, P.; Wei, Z.; Siuzdak, K.; Kouame, N.A.; Kowalska, E.; Remita, H.; Zaleska-Medynska, A. Enhanced photocatalytic, electrochemical and photoelectrochemical properties of TiO_2 nanotubes arrays modified with Cu, AgCu and Bi nanoparticles obtained via radiolytic reduction. *Appl. Surf. Sci.* **2016**, *387*, 89–102. [CrossRef]
34. Zong, M.; Bai, L.; Liu, Y.; Wang, X.; Zhang, X.; Huang, X.; Hang, R.; Tang, B. Antibacterial ability and angiogenic activity of Cu-Ti-O nanotube arrays. *Mater. Sci. Eng. C* **2017**, *71*, 93–99. [CrossRef]
35. Kim, D.; Fujimoto, S.; Schmuki, P.; Tsuchiya, H. Nitrogen doped anodic TiO_2 nanotubes grown from nitrogen-containing Ti alloys. *Electrochem. Commun.* **2008**, *10*, 910–913. [CrossRef]
36. He, J.-B.; Lu, D.-Y.; Jin, G.-P. Potential dependence of cuprous/cupric duplex film growth on copper electrode in alkaline media. *Appl. Surf. Sci.* **2006**, *253*, 689–697. [CrossRef]
37. Jiang, X.; Herricks, T.; Xia, Y. CuO Nanowires Can Be Synthesized by Heating Copper Substrates in Air. *Nano Lett.* **2002**, *2*, 1333–1338. [CrossRef]
38. Mazierski, P.; Nadolna, J.; Lisowski, W.; Winiarski, M.J.; Gazda, M.; Nischk, M.; Klimczuk, T.; Zaleska-Medynska, A. Effect of irradiation intensity and initial pollutant concentration on gas phase photocatalytic activity of TiO_2 nanotube arrays. *Catal. Today* **2017**, *284*, 19–26. [CrossRef]
39. Roy, P.; Berger, S.; Schmuki, P. TiO_2 Nanotubes: Synthesis and Applications. *Angew. Chem. Int. Ed.* **2011**, *50*, 2904–2939. [CrossRef]

40. Regonini, D.; Bowen, C.R.; Jaroenworaluck, A.; Stevens, R. A review of growth mechanism, structure and crystallinity of anodized TiO_2 nanotubes. *Mater. Sci. Eng. R Rep.* **2013**, *74*, 377–406. [CrossRef]
41. Grimes, C.A.; Mor, G.K. *TiO_2 Nanotube Arrays: Synthesis, Properties, and Applications*; Springer: Dordrecht, The Netherlands; New York, NY, USA, 2009; ISBN 978-1-4419-0067-8.
42. Valota, A.; LeClere, D.J.; Hashimoto, T.; Skeldon, P.; Thompson, G.E.; Berger, S.; Kunze, J.; Schmuki, P. The efficiency of nanotube formation on titanium anodized under voltage and current control in fluoride/glycerol electrolyte. *Nanotechnology* **2008**, *19*, 355701. [CrossRef]
43. Biesinger, M.C.; Lau, L.W.M.; Gerson, A.R.; Smart, R.S.C. Resolving surface chemical states in XPS analysis of first row transition metals, oxides and hydroxides: Sc, Ti, V, Cu and Zn. *Appl. Surf. Sci.* **2010**, *257*, 887–898. [CrossRef]
44. Naumkin, A.V.; Kraut-Vass, A.; Gaarenstroom, S.W.; Powell, C.J. NIST X-ray Photoelectron Spectroscopy Database. 2012. Available online: https://srdata.nist.gov/xps/ (accessed on 4 June 2018).
45. Suzuki, S.; Hirabayashi, K.; Mimura, K.; Okabe, T.; Isshiki, M.; Waseda, Y. Surface Layer Formed by Selective Oxidation in High-Purity Copper-Titanium Binary Alloys. *Mater. Trans.* **2002**, *43*, 2303–2308. [CrossRef]
46. Sanguinetti, S.; Guzzi, M.; Gurioli, M. Accessing structural and electronic properties of semiconductor nanostructures via photoluminescence. In *Characterization of Semiconductor Heterostructures and Nanostructures*; Elsevier: New York, NY, USA, 2008; pp. 175–208. ISBN 978-0-444-53099-8.
47. Liqiang, J.; Yichun, Q.; Baiqi, W.; Shudan, L.; Baojiang, J.; Libin, Y.; Wei, F.; Honggang, F.; Jiazhong, S. Review of photoluminescence performance of nano-sized semiconductor materials and its relationships with photocatalytic activity. *Sol. Energy Mater. Sol. Cells* **2006**, *90*, 1773–1787. [CrossRef]
48. Garlisi, C.; Szlachetko, J.; Aubry, C.; Fernandes, D.L.A.; Hattori, Y.; Paun, C.; Pavliuk, M.V.; Rajput, N.S.; Lewin, E.; Sá, J.; Palmisano, G. N-TiO_2/Cu-TiO_2 double-layer films: Impact of stacking order on photocatalytic properties. *J. Catal.* **2017**, *353*, 116–122. [CrossRef]
49. Beltran-Huarac, J.; Guinel, M.J.-F.; Weiner, B.R.; Morell, G. Bifunctional Fe_3O_4/ZnS:Mn composite nanoparticles. *Mater. Lett.* **2013**, *98*, 108–111. [CrossRef]
50. Mazierski, P.; Malankowska, A.; Kobylański, M.; Diak, M.; Kozak, M.; Winiarski, M.J.; Klimczuk, T.; Lisowski, W.; Nowaczyk, G.; Zaleska-Medynska, A. Photocatalytically Active TiO_2/Ag_2O Nanotube Arrays Interlaced with Silver Nanoparticles Obtained from the One-Step Anodic Oxidation of Ti–Ag Alloys. *ACS Catal.* **2017**, *7*, 2753–2764. [CrossRef]
51. Park, S.-M.; Razzaq, A.; Park, Y.H.; Sorcar, S.; Park, Y.; Grimes, C.A.; In, S.-I. Hybrid Cu_xO–TiO_2 Heterostructured Composites for Photocatalytic CO_2 Reduction into Methane Using Solar Irradiation: Sunlight into Fuel. *ACS Omega* **2016**, *1*, 868–875. [CrossRef]
52. Zhang, Z.; Wang, P. Highly stable copper oxide composite as an effective photocathode for water splitting via a facile electrochemical synthesis strategy. *J. Mater. Chem.* **2012**, *22*, 2456–2464. [CrossRef]
53. Luna, A.L.; Valenzuela, M.A.; Colbeau-Justin, C.; Vázquez, P.; Rodriguez, J.L.; Avendaño, J.R.; Alfaro, S.; Tirado, S.; Garduño, A.; De la Rosa, J.M. Photocatalytic degradation of gallic acid over CuO–TiO_2 composites under UV/Vis LEDs irradiation. *Appl. Catal. A Gen.* **2016**, *521*, 140–148. [CrossRef]
54. Chen, L.; Tang, M.; Chen, C.; Chen, M.; Luo, K.; Xu, J.; Zhou, D.; Wu, F. Efficient Bacterial Inactivation by Transition Metal Catalyzed Auto-Oxidation of Sulfite. *Environ. Sci. Technol.* **2017**, *51*, 12663–12671. [CrossRef]
55. Stephens, C. Bacterial sporulation: A question of commitment? *Curr. Biol.* **1998**, *8*, R45–R48. [CrossRef]
56. Grossman, A.D.; Losick, R. Extracellular control of spore formation in *Bacillus subtilis*. *Proc. Natl. Acad. Sci. USA* **1988**, *85*, 4369–4373.
57. Setlow, P. Germination of Spores of Bacillus Species: What We Know and Do Not Know. *J. Bacteriol.* **2014**, *196*, 1297–1305. [CrossRef]
58. Jacoby, W.A.; Maness, P.C.; Wolfrum, E.J.; Blake, D.M.; Fennell, J.A. Mineralization of Bacterial Cell Mass on a Photocatalytic Surface in Air. *Environ. Sci. Technol.* **1998**, *32*, 2650–2653. [CrossRef]
59. Saito, T.; Iwase, T.; Horie, J.; Morioka, T. Mode of photocatalytic bactericidal action of powdered semiconductor TiO_2 on mutans streptococci. *J. Photochem. Photobiol. B Biol.* **1992**, *14*, 369–379. [CrossRef]
60. Kikuchi, Y.; Sunada, K.; Iyoda, T.; Hashimoto, K.; Fujishima, A. Photocatalytic bactericidal effect of TiO_2 thin films: Dynamic view of the active oxygen species responsible for the effect. *J. Photochem. Photobiol. A Chem.* **1997**, *106*, 51–56. [CrossRef]

61. Kunicki-Goldfinger, W.; Baj, J.; Markiewicz, Z.; Kobyliński, S. *Życie Bakterii*; Wydawnictwo Naukowe PWN: Warszawa, Poland, 2008; ISBN 978-83-01-14378-7.
62. Bubacz, K.; Kusiak-Nejman, E.; Tryba, B.; Morawski, A.W. Investigation of OH radicals formation on the surface of TiO_2/N photocatalyst at the presence of terephthalic acid solution. Estimation of optimal conditions. *J. Photochem. Photobiol. A Chem.* **2013**, *261*, 7–11. [CrossRef]